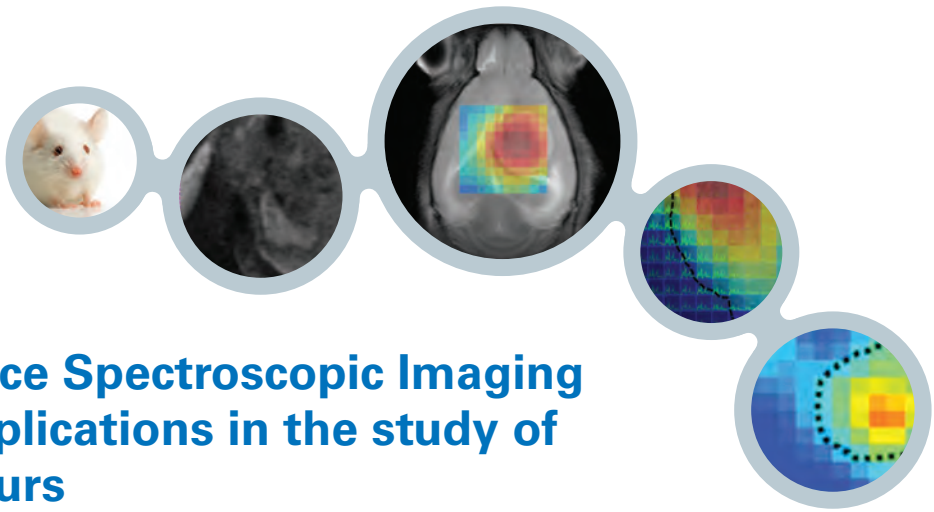

Magnetic Resonance Spectroscopic Imaging acquisition and applications in the study of mouse brain tumours

Delgado-Goñi T[1,2], Simões RV[1,2,5], Lope-Piedrafita S[3,2], Arús C[1,2,4].

[1]Dept. Bioquímica i Biologia Molecular, Universitat Autònoma de Barcelona, Unitat de Biociències, Edifici C, 08193 Cerdanyola del Vallès, Spain.

[2]Centro de Investigación Biomédica en Red en Bioingeniería, Biomateriales y Nanomedicina (CIBER-BBN), Cerdanyola del Vallès, Spain.

[3]Servei de RMN, Universitat Autònoma de Barcelona, Edifici C, 08193 Cerdanyola del Vallès, Spain.

[4]Institut de Biotecnologia i de Biomedicina. Universitat Autònoma de Barcelona. Spain.

[5] Present Address: Dept. Medical Physics, Memorial Sloan-Kettering Cancer Center, 10021 New York, NY, USA.

Summary

MRSI acquisition from preclinical brain tumours in mice (glioblastoma and oligodendroglioma) can be properly performed in a 7T Biospec® MR system in approximately 20 minutes per echo time (12 and 136 ms) with the CSI method using PRESS localization. FASTMAP shimming produces the required B0 field homogeneity. Initial processing before exporting can be carried out with the Paravision 5.0 software. Further post-processing with other software: 3dCSI, DMPM, SC2.0 and associated modules, can produce average spectra from selected regions, molecular images of selected peak heights or even nosologic-like tissue type images. Applications of this strategy are illustrated for brain tumours, but should not be limited to them.

Introduction

One of the most promising non-invasive methods for supporting MRI and radiology in the diagnosis of several diseases is ^{1}H-MRS [(1)]. Single voxel (SV) MRS allows measuring the biochemical content of living tissues and provides metabolic information complementary to anatomical changes found in radiological and MRI exams [(2–4)]. In addition, magnetic resonance spectroscopic imaging (MRSI), provides metabolic information which can be processed and presented as density maps of several metabolites from humans or preclinical models [(5)], allowing, for example, the differentiation of tumour grade and spatial metabolic heterogeneity inside brain tumours, and the delimitation of regions with metabolic abnormalities [(6,7)]. MRSI allows the study of large regions enclosing the lesion and this information is very useful for delineating the border of the tumour for neurosurgery purposes and for determining cell infiltration before selecting an appropriate radiotherapy protocol [(8)]. The detectability of infiltration is also related to the concentration of infiltrating cells and to the uniqueness and relative amount of the infiltration biomarker used, e.g. detection of mobile lipids in an apparently normal brain parenchyma region would immediately suggest possible infiltration.

Constant improvement and refinement in MRSI techniques, including higher magnetic field strength magnets and better methods of data acquisition and processing, have improved both spatial and temporal resolution in recent years. High magnetic fields provide higher sensitivity and better spectral resolution. Very efficient localized shimming approaches, like Fastmap and Mapshim [9,10], have been developed to optimize the static B0 field homogeneity in a straightforward manner. Good shimming is a prerequisite for successful MRSI in order to have good water suppression, narrow spectral peaks and to minimize image distortion. Outer volume saturation (OVS) techniques are also a standard feature on most MR scanners and are required for good MRSI. As for data acquisition, several approaches have been implemented- like elliptical, circular or Hanning-weighted k-space sampling schemes- for improving the point spread function while maintaining or reducing the total experiment duration. The main goal of this report is to illustrate the application of MRSI to produce molecular images of preclinical brain tumours: glioblastoma (GBM, grade IV) and oligodendroglioma (ODG, grade II), using their spectroscopic profile, and the utility of Perturbation Enhanced MRSI (PE-MRSI) for tumour characterization.

Material and Methods

Ten female C57BL/6 mice, 20–22g weight, were obtained from Charles River Laboratories (France) and were housed at the Universitat Autònoma de Barcelona animal facility (Cerdanyola del Vallès, Spain). The S100β-v-erbB/Ink4a-Arf(+/-) Genetically Engineered Mice (GEM) model was obtained from the MMHCC, NCI-Frederick, USA repository and housed at the same facility. Two GEM (ODG II) were then included in this study. All animal studies were approved by the local ethics committee, according to the regional and state legislation (protocol DMAH-4600; CEEAH-1176).

C57BL/6 animals were inoculated with GL261 glioma cells (105 in 4µl of RPMI culture media) by stereotactic intracranial injection into the striatum of the right hemisphere, as described in [11].

MRSI experiments were performed at 7 Tesla in a Bruker Biospec 70/30 USR equipped with a B-GA 12 gradient coil inserted into the standard B-GA 20 S gradient coil set up. This high-performance spectrometer hardware provides gradient strengths of 400 mT/m with slew rates of 5,500 T/m/s and rise times of 80 microseconds, and has high shim currents giving shim strengths up to 240 Hz/cm^2/A. High duty cycles are used to minimize B0 field drift due to temperature variations that could be caused by those high shim currents. A 7.2 cm inner diameter volume coil was used for excitation together with a dedicated mouse brain quadrature ^{1}H surface coil, with a shape adapted to the mouse head for an optimal B1 homogeneity and sensitivity in the area of the brain, for signal reception.

Animals were placed in a mouse bed and anesthetised with isoflurane 0.5–1.5% in O_2, keeping their respiratory frequency between 60–80 breaths/min during MRI scans. A recirculating water-system, incorporated in the animal bed, was used to control the body temperature, measured by a rectal probe and kept between 37–38°C, unless otherwise indicated. Breathing and temperature were constantly monitored (SA Instruments, Inc., New York, USA).

Six animals were used for MRSI studies. Two reference high-resolution T2W images, with different TE (36 and 132 ms respectively), and 12 ms and 136 ms TE basal MRSI were acquired. Acquisition parameters for T2w sequences were: echo train length, 8; field of view (FOV), 17.6 x 17.6 mm; matrix (MTX), 256 x 256 (75 x 75 µm/pixel); number of slices (NS), 1; slice thickness (ST), 1 mm; TR, 3000 ms: TE, 36 and 132 ms; number of averages (NA), 3; total acquisition time (TAT), 3 min and 36 sec.

MRSI experiments were acquired using a 2D CSI (Chemical Shift Imaging) sequence with PRESS localization, FOV, 17.6 x 17.6 mm; Volume of Interest (VOI), 5.5 x 5.5 x 1.0 mm, positioned such that most of the tumour and part of the nearby normal/peritumoral brain parenchyma were included; ST, 1 mm; TR, 2500 ms; SW, 4006.41 Hz; 512 NEX; TAT, 21 m 30s. Water suppression was performed with VAPOR and linear and second order shims were automatically adjusted with FASTMAP in a 5.8 x 5.8 x 5.8 mm volume which contained the VOI region. Six saturation slices (ST,10 mm; sech-shaped pulses: 1.0 ms/20250 Hz) were positioned around the VOI to minimize outer volume contamination in the signals obtained. Spatial resolution was defined by a 8 x 8 voxel matrix over the FOV (4.84 µl nominal resolution) reconstructed after Fourier interpolation to a 32 x 32 matrix, as described in [12]. After the studies were completed, mice were sacrificed with an i.p. injection of pentobarbital (200 mg/Kg, 60 mg/ml). ODG afflicted-mice brains were collected, fixed in 4% formaldehyde and analysed by histopathology (H&E staining) in order to obtain the tumour diagnosis.

Four animals were used for Perturbation-Enhanced-MRSI (PE-MRSI) studies. Their body temperature was stabilised to 28.5–29.5 °C, 45 min after inducing anaesthesia, because moderate brain hypothermia (~30°C) has been reported to be a necessary requirement in the GL261 tumour model in order to maximize the hyperglycemia-induced pattern perturbation [12]. MRSI sequence parameters were the same described above. Two reference MRSI scans were initially acquired, one with short echo time (12 ms TE), followed by another one at long echo time (136 ms TE). At this point (90 min after induction of anesthesia), acute hyperglycemia was induced by an i.p. bolus injection of 10 mL/g D-glucose 25% (w/v) in saline (1.4 M)[11]. Five consecutive short TE MRSI scans were then acquired.

MRSI grid spectra were processed in the Bruker's CSI Dashboard Tool software (within Paravision v 5.0, figure 1), with an exponential line broadening of 4 Hz. First-order phase correction was performed in the central spectrum of the grid and then applied to the rest. The 2dseq files from Bruker were post-processed with the 3diCSI software [13] in order to obtain text files containing all the information acquired with MRSI sequences, including apodization and phase correction. These text files were processed with the software developed in our group, the Dynamic MRSI Processing Module (DMPM) [14], which runs some scripts in Matlab for normalising each spectrum to unit length (UL2) and converting the text files to color-coded maps representing the relative intensities of the user-selected metabolites (e.g. mobile lipids (ML) + lactate at 1.3 ppm or glucose+taurine at 3.43 ppm).

Figure 1

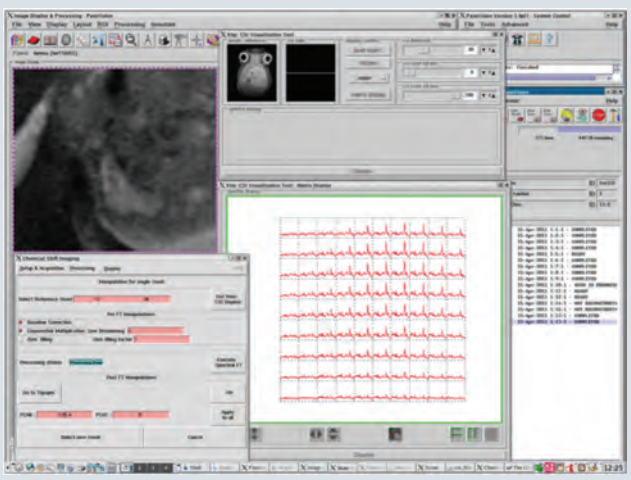

Paravision 5.0 CSI visualization Tool and CSI Dashboard Tool software. On the top left corner, there is a T2w image corresponding to the VOI selected for MRSI acquisition in a GL261 tumour. Under this image, the MRSI fid processing window is displayed. On the middle top, the visualization window is shown and under it, the MRSI grid (10 x 10) obtained after post-processing an MRSI data matrix.

Results and Discussion

All tumours were clearly visible and well defined in the high-resolution T2w images used as references for MRSI acquisition (see two representative examples in Figure 2). The shimming performed with the FASTMAP procedure before MRSI acquisition provided good quality spectra with a linewidth below 20–22 Hz for tissue water in all cases. The MRSI spectra obtained showed a good signal to noise ratio (considering a threshold of 7.8). Figure 1 shows a screen-shot of the Paravision 5.0 MRSI processing module.

In Figure 2, the mean spectra from a GL261 GBM (grade IV) and an ODG (grade II) are extracted from the tumour voxels selected from their respective MRSI grids (VOI) and compared. A visual analysis of the average tumour spectral pattern reveals for example that the ratio choline/creatine (3.21/3.03 ppm) is clearly higher in the GBM, than in the ODG-II. Mobile Lipids (ML) resonances at 0.9 ppm and ML+Lactate at 1.3 ppm also reach high levels in both tumours.

Figure 2

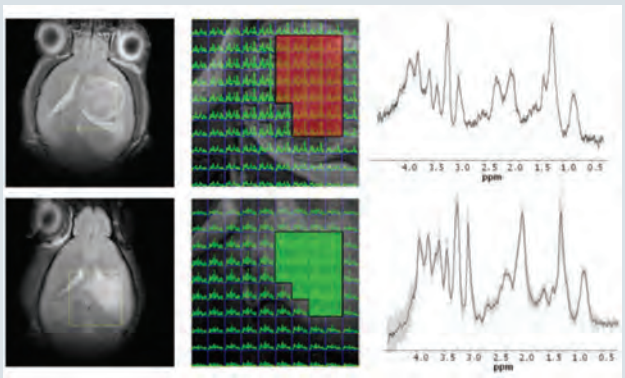

MRSI acquisitions from brain tumours of different type and grade and their respective mean spectra (normalised to UL2) calculated from some of the voxels in the VOI. On the top row, data from a representative GL261 GBM are shown and, in the bottom row, data from a representative ODG-II are displayed. From left to right: High-resolution T2w images from tumour afflicted mice with the acquisition VOI marked with a yellow line. VOIs from both tumours containing their respective spectral grid for (10 x 10 voxels). Some of the GBM spectra are selected in red colour and some of the ODG-II in green colour. Mean spectra (SD in gray shading, obtained using a homemade script in R software v 2.6.1.) from both type of tumours acquired at short TE (12 ms), in the range of 0.5 to 4.5 ppm are shown in the right column.

Figure 3

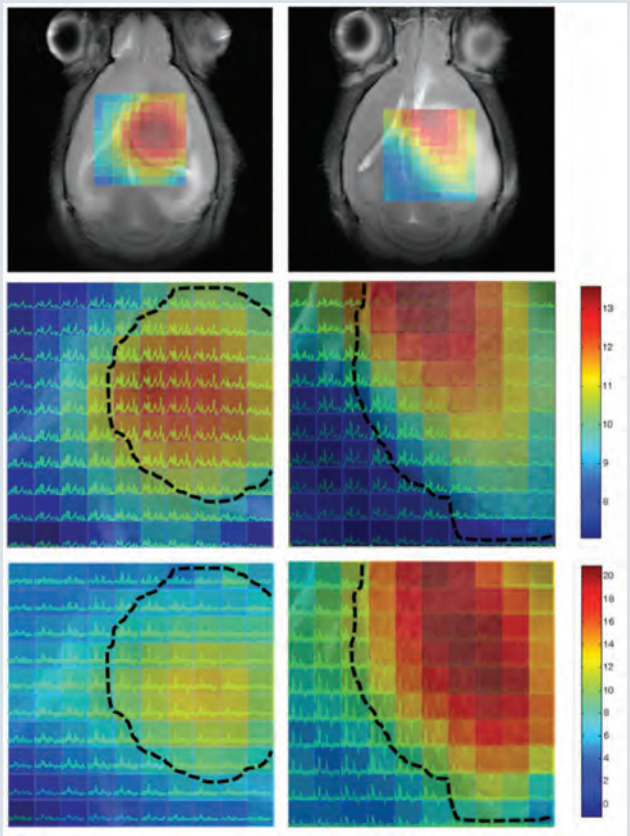

On the top row, ML+Lactate maps acquired from spectra signal heights (TE 12 ms) at 1.3 ppm, superimposed to the high resolution T2w reference images of a GBM (on the left) and an ODG-II (on the right). The expanded colour coded maps (normalised to UL2) representing ML peak heights at 1.3 ppm are shown in the second row. T2w-defined tumour boundaries are drawn with a black dotted line on the maps, and the relative intensity colour-coded scale is shown at the right edge of the image. On the bottom row, Lactate maps acquired from spectral signal heights at 1.3 ppm in TE 136 ms MRSI spectra.

The differences detected at average spectra level in both cases can be evaluated for shape or heterogeneity in the metabolic profile of both tumours, generating colour coded maps for the metabolites of interest (Figure 3). These maps represent the normalized intensity of one metabolite selected from the spectral pattern (Lactate or ML+Lactate for example), in all the voxels contained in the VOI, both tumour and surrounding brain parenchyma. In the case of mice with brain tumours, ML+ Lactate signals are high as expected inside the tumour with higher apparent heterogeneity in the ODG. In the case of Lactate, analysed in MRSI spectra acquired with 136 ms of TE, the highest signal intensity is also detected inside the tumour in both cases, but is clearly higher inside the ODG-II in comparison with the GBM. This kind of differences may be of interest in further analysis for tumour spectral pattern discrimination.

Further pattern recognition-based data analysis of these MRSI grids can produce "nosologic-like" tumour type images [15,16].

The metabolic maps obtained from MRSI sequences can be implemented by acquiring MRSI VOIs after inducing a metabolic perturbation of the basal tumour spectral pattern. Glucose injection is an example of this kind of challenge, because this compound is well known as the major substrate for cerebral metabolism in both man and animals and is consumed by the tumour[17]. Figure 4 shows the different glucose accumulation in three parts of the MRSI VOI at four time-points after injection. The peritumoral/normal brain parenchyma does not seem to be affected, but glucose+taurine signal intensity (3.43 ppm) clearly changes along time. Moreover, the two spatial regions studied inside the GBM respond in a different way to the glucose challenge, which may be due to spatial heterogeneities in the tumoral tissue and may be used in further studies for a better characterisation of the tumour mass.

Figure 4

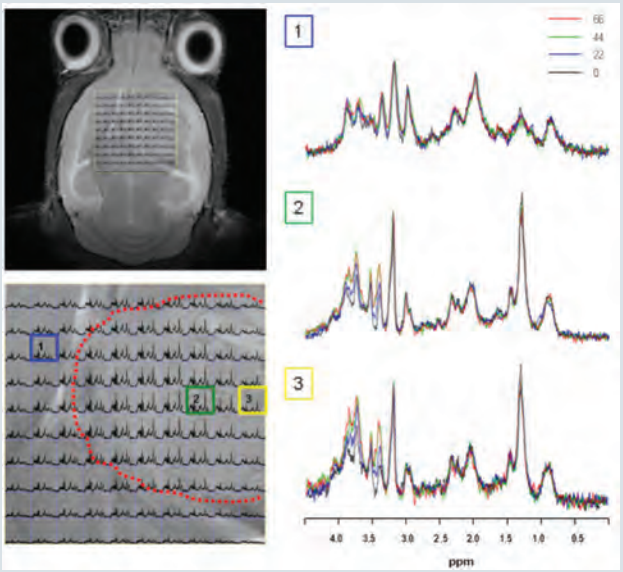

On the left column, a high resolution T2w reference image with the VOI selected for MRSI studies in a GL261 GBM is shown on the top. On the bottom the MRSI grid acquired with short TE (12 ms). The tumour boundary is drawn with a red dotted line. Three different regions of the VOI are selected with squares: 1-normal/peritumoral brain parenchyma; 2-Tumour centre; 3- Tumour edge. On the right column, spectra acquired from these three spatial regions at four different time-points after glucose injection (time-points in minutes are described in the colour legend on the top corner at right) are represented. The signal intensity increase at 3.43 ppm is clearly visible for regions 2 and 3, both inside the tumour (Adapted from [12]).

Figure 5

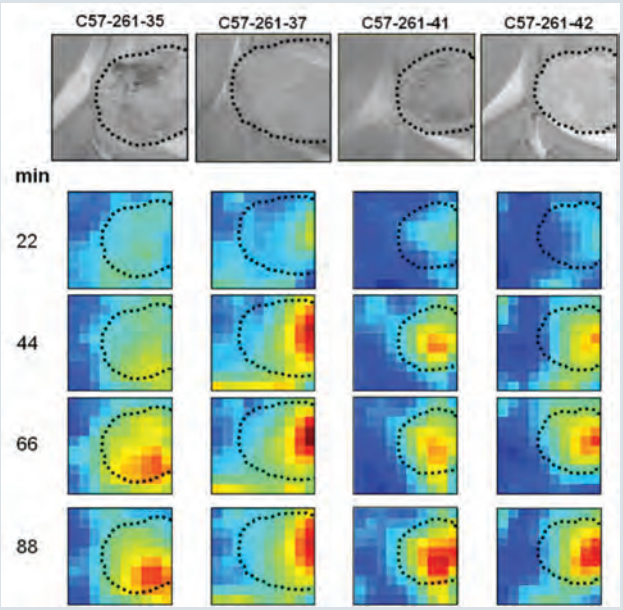

On the top row, high resolution T2w images corresponding to the VOIs selected for PE-MRSI studies in four GL261 tumour bearing mice. The next four rows show the colour-coded maps representing four time-points after glucose injection, indicated on the left column. Each column contains the colour-coded maps for glucose signal intensity of one animal (represented on the first row) at different times. Glucose signal enhancement is visible inside the four tumours. The maximum intensity is reached at a different time-point depending on the animal and hot-spots suggest heterogeneity in glucose consumption in different tumour regions (Adapted from [12]).

The differences shown at a spectral level in Figure 4 can be translated to differences in colour coded maps obtained from these MRSI sequences. In Figure 5, the colour coded maps represented correspond to Glucose signal increase in intensity at four different time-points after injection in the four animals used in the study. They confirm the differences observed in Figure 4: glucose accumulation is clearly higher inside the tumours. Hot-spots of maximum accumulation are shown inside the tumour mass, which suggest different metabolic profiles inside this tissue, possibly related to differences in glucose consumption in different regions of the tumour. Once more, all this information may be useful for pattern recognition-based data analysis.

Acknowledgements

Work supported by: Ministerio de Ciencia e Innovación, MICINN (Spain), SAF 2008-03323; Centro de Investigación Biomédica en Red – Bioingeniería Biomateriales y Nanomedicina (CIBER-BBN) and the intramural project PROGLIO, an initiative of the Instituto de Salud Carlos III (Spain), co-funded with EU FEDER funds. Authors thank Sandra Ortega-Martorell and Margarida Julià-Sapé for help in the use and adaptation of the SpectraClassifier software and associated modules.

References

1. Kwock L, Smith JK, Castillo M, Ewend MG, Collichio F, Morris DE, Bouldin TW, Cush S. Clinical role of proton magnetic resonance spectroscopy in oncology: brain, breast, and prostate cancer. Lancet Oncol 2006;7(10):859-868.
2. Fellows GA, Wright AJ, Sibtain NA, Rich P, Opstad KS, McIntyre DJ, Bell BA, Griffiths JR, Howe FA. Combined use of neuroradiology and ^{1}H-MR spectroscopy may provide an intervention limiting diagnosis of glioblastoma multiforme. J Magn Reson Imaging;32(5):1038-1044.
3. Majos C, Alonso J, Aguilera C, Serrallonga M, Perez-Martin J, Acebes JJ, Arus C, Gili J. Proton magnetic resonance spectroscopy ((1)H MRS) of human brain tumours: assessment of differences between tumour types and its applicability in brain tumour categorization. Eur Radiol 2003;13(3):582-591.
4. Sibtain NA, Howe FA, Saunders DE. The clinical value of proton magnetic resonance spectroscopy in adult brain tumours. Clin Radiol 2007;62(2):109-119.
5. Le HC, Lupu M, Kotedia K, Rosen N, Solit D, Koutcher JA. Proton MRS detects metabolic changes in hormone sensitive and resistant human prostate cancer models CWR22 and CWR22r. Magn Reson Med 2009;62(5):1112-1119.
6. Simonetti AW, Melssen WJ, van der Graaf M, Postma GJ, Heerschap A, Buydens LM. A chemometric approach for brain tumor classification using magnetic resonance imaging and spectroscopy. Anal Chem 2003;75(20):5352-5361.
7. Chuang CF, Chan AA, Larson D, Verhey LJ, McDermott M, Nelson SJ, Pirzkall A. Potential value of MR spectroscopic imaging for the radiosurgical management of patients with recurrent high-grade gliomas. Technol Cancer Res Treat 2007;6(5):375-382.
8. Martinez-Bisbal MC, Celda B. Proton magnetic resonance spectroscopy imaging in the study of human brain cancer. Q J Nucl Med Mol Imaging 2009;53(6):618-630.
9. Grütter R. Automatic, localized in Vivo adjustment of all first- and second-order shim coils. Magnetic Resonance in Medicine 1993;29(6):804-811.
10. Kanayama S, Kuhara S, Satoh K. In vivo rapid magnetic field measurement and shimming using single scan differential phase mapping. Magn Reson Med 1996;36(4):637-642.
11. Simoes RV, Garcia-Martin ML, Cerdan S, Arus C. Perturbation of mouse glioma MRS pattern by induced acute hyperglycemia. NMR Biomed 2008;21(3):251-264.
12. Simoes RV, Delgado-Goni T, Lope-Piedrafita S, Arus C. ^{1}H-MRSI pattern perturbation in a mouse glioma: the effects of acute hyperglycemia and moderate hypothermia. NMR Biomed 2010;23(1):23-33.
13. http://mrs.cpmc.columbia.edu/3dicsi.html.
14. http://gabrmn.uab.es/DMPM.
15. Ortega-Martorell S, Olier I, Julia-Sape M, Arus C. SpectraClassifier 1.0: a user friendly, automated MRS-based classifier-development system. BMC Bioinformatics 2010;11:106.
16. Simoes RV, Ortega-Martorell S, Delgado-Goni T, Le Fur J, Pumarola M, Candiota AP, Martín J, Stoyanova R, Cozzone PJ, Julià-Sapé M, Arús C. Improving the classification of brain tumors in mice with perturbation enhanced (PE)-MRSI. Integr Biol (Camb). 2012; 4(2):183-191.
17. Ziegler A, von Kienlin M, Decorps M, Remy C. High glycolytic activity in rat glioma demonstrated in vivo by correlation peak ^{1}H magnetic resonance imaging. Cancer Res 2001;61(14):5595-5600.

www.bruker-biospin.com

Bruker BioSpin

info@bruker-biospin.com